# Analytic Damping Model for a Square Perforation Cell

Timo Veijola

Helsinki University of Technology, P.O.Box 3000, FIN-02015 HUT, Finland,
E-mail:timo.veijola@hut.fi

## ABSTRACT

A model for damping due to gas flow in a perforation cell is presented. The cell is a volume around a single hole of a perforated squeezed-film damper. Here, the perforations are holes with square cross-sections. The model is derived partly from analytic expressions for flow resistances of long microchannels, partly from FEM simulations. First, 2D simulations with a Reynolds solver are performed to solve the flow resistance in the air gap regime. Then, 3D Navier-Stokes simulations are performed to characterize the intermediate regime below the perforation, the perforation itself, and the gas outflow regime above the perforation. Slip flow boundary conditions are used to make the model applicable in MEMS structures.

Fitting techniques are applied and the flow resistance of the perforation cell is expressed as a set of simple equations. The model is verified against 3D FEM simulations of a perforated damper with 4...64 square holes.

***Keywords***: perforation, compact model, square hole, Reynolds equation, slip flow

## 1 INTRODUCTION

Perforated squeezed-film damper structures are used in several MEMS applications to control the amount of damping due to the surrounding gas. To simulate the damping characteristics, FEM tools can be used to solve the gas flow in the damper and around it. Unfortunately, full 3D simulation of the Navier-Stokes equation are, in practice, impossible due to the huge number of elements needed. Additionally, accurate modeling of the damping requires the consideration of rare-gas flow inside the damper and around it. Order reduction utilizing a local impedance profile has been studied [1], but without rare gas and edge effects. A mixed-level approach has also been published [2]. Analytic models are restricted to simple modes of motion and homogenous perforation [3], [4], [5]. Analytic models for perforation cells have been presented in the literature [6], [3], [7], [8], and [2].

We have developed a model for a *perforation cell* [9] for holes having a circular cross-section. In [9], we approximated holes with a square cross-section with these cylindrical perforation cells with moderate accuracy. To improve the accuracy of the damping model for square perforations, a novel model for a square perforation cell is derived in this paper.

The method used is similar to the one used for circular perforations in [9]: analytic flow resistance models are combined with results from FEM simulations. The challenge here is that 3D simulations are needed instead of (axisymmetric) 2D simulations. Moreover, additional simulations with a Reynolds solver are needed in characterizing the flow in the air gap.

## 2 PERFORATION CELL

Figure 1 shows the topology of the square perforation cell. It is assumed that the side of this cell is $s_x$ (perforation pitch) and the side of the square hole is $s_0$.

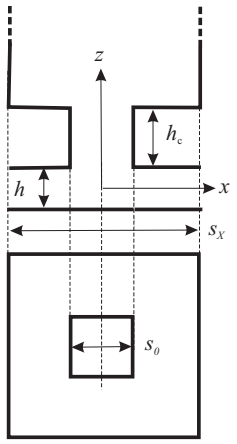


Figure 1: Topology of the square perforation cell.

### 2.1 Flow Resistances in the Perforation Cell

The analytic model derived in this paper consists of two main parts for the two regions in the perforation cell: the squeezed-film region in the air gap and the capillary flow in the perforation. Two additional regions can be distinguished: one is the intermediate region in the air gap under the hole, and the other is the outflow region above the hole.

The flow in each region is modeled with lumped flow resistances. The resulting model consists of six flow resistances, as illustrated in Fig. 2. The mechanical resistance $R_\mathrm{P}$ of the perforation cell is

$$R_\mathrm{P} = R_\mathrm{S} + R_\mathrm{IS} + R_\mathrm{IB} + \frac{s_\mathrm{x}^4}{s_0^4}\left(R_\mathrm{IC} + R_\mathrm{C} + R_\mathrm{E}\right). \qquad (1)$$

Only the resistance $R_\mathrm{C}$ is derived analytically, all others are derived from FEM simulations. Resistance $R_\mathrm{S}$ is derived from simulations with a Reynolds solver and the remaining resistances are derived from 3D simulations of the perforation cell with a Navier-Stokes solver.

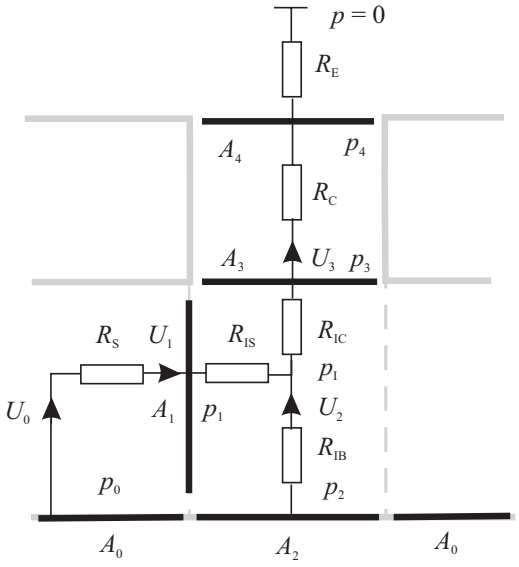


Figure 2: The lumped flow resistances needed in the perforation cell model.

## 2.2 Squeezed-film Region

For a cylindrical perforation cell, the flow from the air gap into the perforation has been modeled by Skvor [6]. Skvor's original formula for the mechanical resistance is

$$R_\mathrm{S} = \frac{12\pi\eta r_\mathrm{x}^4}{Q_\mathrm{ch} h^3}\left(\frac{1}{2}\ln\frac{r_\mathrm{x}}{r_0} - \frac{3}{8} + \frac{r_0^2}{2r_\mathrm{x}^2} - \frac{r_0^4}{8r_\mathrm{x}^4}\right), \qquad (2)$$

where $r_\mathrm{x}$ and $r_0$ are the outer and inner radii of the cylindrical perforation cell, respectively. In Eq. (2) the relative flow rate coefficient $Q_\mathrm{ch} = 1 + 6K_\mathrm{ch}$, where $K_\mathrm{ch} = \lambda/h$, includes the slip correction due to the flow profile for rare gas.

Skvor's equation is used here for the square cell, and the relation between $r_0$ and $r_\mathrm{x}$ to $s_0$ and $s_\mathrm{x}$ is derived from FEM simulations with the Reynolds solver in section 3.

## 2.3 Perforation and Gas Outlet

When the hole diameter is comparable with the gap height, the flow resistance of the hole becomes important. In many practical cases, the holes are relatively short, and the end-effects become important as well. Especially for a rare gas, these end-effects become relatively strong: the slip between the channel wall and gas is strongly dependent on the Knudsen number, whereas the flow resistance of the elongation depends less on it.

Models for short capillaries with rare gas effects have been published [10], [11], but here the outlet conditions are different. Here, the flow resistance of a short capillary is modeled with a sum of two resistances: the resistance $R_\mathrm{C}$ of a long square channel (with slip conditions) and an open end resistance $R_\mathrm{E}$ having an effective a length of $\Delta_\mathrm{E} s_0$ [11]:

$$R_\mathrm{C} + R_\mathrm{E} = 28.454\eta\left(\frac{h_\mathrm{c}}{Q_\mathrm{sq}} + \Delta_\mathrm{E} s_0\right), \qquad (3)$$

where $h_\mathrm{c}$ is the length of the hole, $\Delta_\mathrm{E}$ is the relative elongation of the channel (one end only) and $Q_\mathrm{sq}$ is the relative flow rate coefficient. In the slip flow regime [12] $Q_\mathrm{sq} = 1 + 7.567K_\mathrm{sq}$, where $K_\mathrm{sq} = \lambda/s_0$ . The elongation $\Delta_\mathrm{E}$ is dependent, both, on the geometry of the structure of the outlet and on the Knudsen number $K_\mathrm{sq}$. In section 3, $\Delta_\mathrm{E}$ is extracted from FEM simulations.

## 2.4 Intermediate Region

The flow resistances of the intermediate region consist of losses due to the changes in the flow profile of the gas entering this region $R_\mathrm{IS}$, and due to the flow turning upwards below the perforation $R_\mathrm{IC}$. No such analytic model exists, and values of these flow resistances are based on channel elongations that will be extracted from FEM simulations. The model presented is formed of two fictitious flow channels that model the end effects of resistances $R_\mathrm{S}$ and $R_\mathrm{C}$ having lengths $\Delta_\mathrm{S} h$ and $\Delta_\mathrm{C} s_0$, respectively.

The value for $R_\mathrm{IS}$ is derived assuming that the additional flow resistance is formed in a wide channel with a width of $w = 4s_0$ (circumference of the hole aperture), height of $h$, and length of $\Delta_\mathrm{S} h$. Since $R_\mathrm{IS}$ is specified as a ratio of the force and velocity at the bottom surface, the flow resistance must be scaled with the square of the ratio of the cross-sectional areas $A_0$ and $A_1$ (see Fig. 2).

$$R_\mathrm{IS} = \frac{12\eta w}{h}\left(\frac{A_0}{A_1}\right)^2 \Delta_\mathrm{S} h = \frac{3\eta(s_\mathrm{x}^2 - s_0^2)^2}{s_0 h^2}\Delta_\mathrm{S}. \qquad (4)$$

The value of $R_\mathrm{IC}$ is the flow resistance of capillary with a square cross-section having a length of $\Delta_\mathrm{C} s_0$.

$$R_\mathrm{IC} = 28.454\eta s_0 \Delta_\mathrm{C}. \qquad (5)$$

In this model $R_\mathrm{IB} = 0$.

## 3 EXTRACTION OF PARAMETERS

To complete the perforation cell model, the effective radii and the relative elongations should be determined. In the following, this data is extracted from FEM simulations.

### 3.1 FEM Simulations

Solvers for the Navier-Stokes equations and the Reynolds equation in a multiphysical FEM software Elmer [13] are used to perform the FEM simulations. Shell scripts are used to automate, both, the geometry generation and the actual simulations.

Parameters for air at atmospheric pressure are used in the simulations, see Table 3.1.

| Symbol | Description | Value | Unit |
|---|---|---|---|
| $P_\mathrm{A}$ | pressure | 101.3 | $10^3\,\mathrm{N/m^2}$ |
| $T_\mathrm{A}$ | temperature | 300 | K |
| $\eta$ | viscosity coefficient | 20 | $10^{-6}\,\mathrm{N\,s/m^2}$ |
| $\lambda$ | mean free path | 69 | $10^{-9}\,\mathrm{m}$ |

Table 1: Gas parameters used in the simulations.

### 3.2 Effective Radii for Skvor's Equation

The Reynolds solver has been used to determine the damping in a square damper with a square hole in the middle. Perpendicular motion is assumed. Zero pressure conditions at the hole are assumed, and at the outer borders the outflow velocity is zero.

A mesh of 20000 elements is used to ensure that the results have sufficient accuracy. $r_\mathrm{x}$ is selected such that the bottom areas of circular and square cells match. This results in

$$r_\mathrm{x} = \frac{s_\mathrm{x}}{\sqrt{\pi}}. \tag{6}$$

It was necessary to make $r_0$ depend on both $s_0$ and $s_\mathrm{x}$. A simple function is formed intuitively, and its coefficients have been determined by fitting.

$$r_0 = \frac{0.58076 s_0}{1 + 0.02108\xi^2 + 0.008\xi^4}, \tag{7}$$

where $\xi = s_0/s_\mathrm{x}$. Figure 3 shows the results of the FEM simulations and the approximation for $R_\mathrm{S}$ at 28 values of the perforation ratio $q$ between 0.25% and 96%. The minimum relative error of the approximation is better than 0.5% for $0 \le q \le 96\,\%$.

### 3.3 Effective Elongations

The Navier-Stokes solver is used to solve the flow in the perforation cell shown in Fig. 1. Due to the symmetry, a quarter of the cell was actually simulated. The surface velocity $v_\mathrm{z}$ was set to 1 m/s, and the force acting

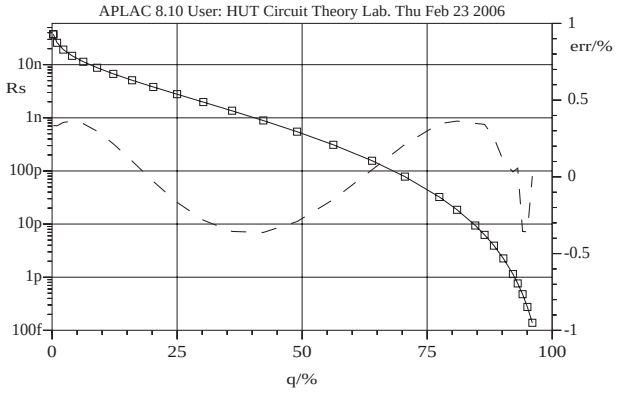


Figure 3: Flow resistance of the air gap in the perforation cell ($5\,\mu\mathrm{m} \times 5\,\mu\mathrm{m}$, $h = 2\,\mu\mathrm{m}$, $Q_\mathrm{ch} = 1$) as a function of the perforation ratio $q = (r_0/r_\mathrm{x})^2 \cdot 100\%$. Results both from FEM simulations with a Reynolds solver (□) and from the approximation $R_\mathrm{S}$ (——) are shown. The relative error of $R_\mathrm{S}$ is also shown (— — —) on the right hand scale.

on the bottom surface was solved. Dimensions $h$, $h_\mathrm{c}$ and $r_0$ were varied, see Table 2. A mesh of 100 000 elements was used.

| Symbol | Description | Value | Unit |
|---|---|---|---|
| $s_\mathrm{x}$ | cell width | 5 | $10^{-6}\,\mathrm{m}$ |
| $s_0$ | hole width | 0.5, 1, …, 4.5 | $10^{-6}\,\mathrm{m}$ |
| $h_\mathrm{c}$ | thickness | 0.5, 1, 2, 5 | $10^{-6}\,\mathrm{m}$ |
| $h$ | air gap height | 1, 2 | $10^{-6}\,\mathrm{m}$ |

Table 2: Dimensions for the simulated perforation cell. 72 different topologies were generated and simulated.

Next, heuristic equations for the elongations were derived, and their coefficients were found by fitting $R_\mathrm{P}$ in Eq. (1) to the FEM simulation results. The resulting functions are:

$$\Delta_\mathrm{S} = 0.122(1 + 6.5\xi - 3.8\xi^2), \tag{8}$$

$$\Delta_\mathrm{C} = 0.302, \tag{9}$$

$$\Delta_\mathrm{E} = 0.242(1 + 4K_\mathrm{sq})(1 - \xi^4)(1 + 0.019\xi^{2.83}), \tag{10}$$

where $\xi = s_0/s_\mathrm{x}$. The maximum relative error in $R_\mathrm{P}$ was below 1 %. Figure 4 compares the fitted model for $R_\mathrm{P}$ against the 3D FEM simulations of the perforation cell.

## 4 VERIFICATION

The novel model has been inserted in the simple model for a square squeezed-film damper (with square perforations), and verified with full 3D simulations of damper structures, see Fig. 5. The simulations and the simple model presented in [9] are reused here.

Figure 6 shows the damping coefficient $R_\mathrm{D}$ for a damper with 64 holes. If the perforation ratio $q$ is less

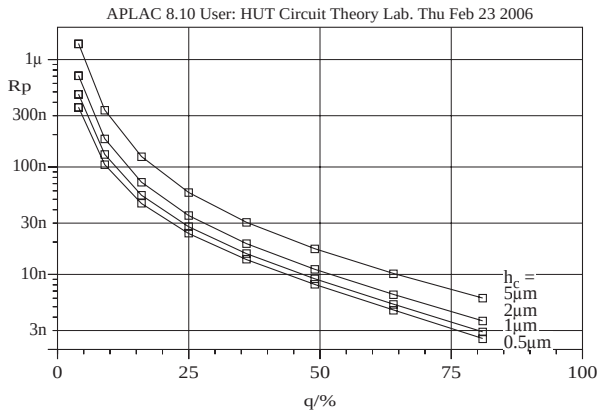


Figure 4: Mechanical resistance of the perforation cell as a function of the perforation ratio. The fitted mode (——) and the result of 3D FEM simulations (□). The air gap height is $h = 1\,\mu$m.

than 65 %, the maximum error is less than 5 %. This is smaller than the 10 % error reported in [9], where cylindrical perforation cell model was used.

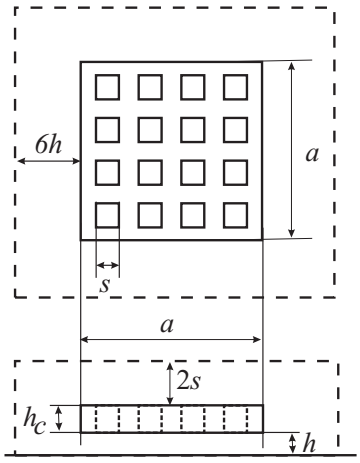


Figure 5: Structure of simulated perforated dampers. Topology with $N = 16$ is shown. Simulation space around the structure is also shown.

## 5 CONCLUSIONS

The presented model can be used to model perforated dampers in various simulation tools, including FEM tools. The implementation is straightforward, since the model contains analytic expressions for the flow resistances. The derived model is valid only for topologies having cell dimensions in the range used here. Since all elongations were extracted in a single phase, the individual flow resistances are not necessary accurately characterized. For a more general model, additional simulations with wider range of dimensions are required.

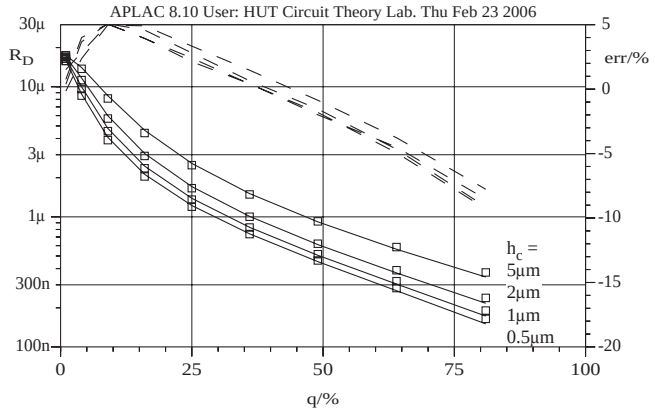


Figure 6: Comparison between the simple perforation damper model (——) with full 3D FEM simulations (□) as a function of the perforation ratio. The relative error (– – –) is also shown on the right hand scale. The number of perforations is 64 and the gap height $h = 1\,\mu$m.

## REFERENCES

[1] Y.-J. Yang and C.-J. Yu *Proceedings of the 5th International Conference on Modeling and Simulation of Microsystems*, (San Juan, PR), pp. 178–181, April 2002.

[2] R. Sattler and G. Wachutka *Proceedings of DTIP 2004*, (Montreux), pp. 377–382, May 2004.

[3] T. Veijola and T. Mattila *Proceedings of Transducers'01*, (Munich, Germany), pp. 1506–1509, June 2001.

[4] M. Bao *et al. Journal of Micromechanics and Microengineering*, vol. 13, pp. 795–800, 2003.

[5] P. Råback *et al. Proceedings of the 6th International Conference on Modeling and Simulation of Microsystems*, vol. 1, (San Francisco), pp. 194–197, February 2003.

[6] Z. Skvor *Acoustica*, vol. 19, pp. 295–299, 1967.

[7] M. Bao *et al. Sensors and Actuators A*, vol. 108, pp. 212–217, 2003.

[8] D. Homentcovschi and R. N. Miles *Journal of the Acoustical Society of America*, vol. 116, pp. 2939–2947, November 2004.

[9] T. Veijola *Microfluidics and Nanofluidics*, vol. 2, no. 2, 2006. In print.

[10] F. Sharipov and V. Seleznev *J. Phys. Chem. Ref. Data*, vol. 27, no. 3, pp. 657–706, 1998.

[11] T. Veijola, "End Effects of Rare Gas Flow in Short Channels and in Squeezed-Film Dampers," *Proceedings of MSM 2002*, (San Juan), April 2002.

[12] W. A. Ebert and E. M. Sparrow *Journal of Basic Engineering, Trans. ASME*, vol. 87, pp. 1018–1024, 1965.

[13] "Elmer – Finite Element Solver for Multiphysical Problems." http://www.csc.fi/elmer.